Nonequilibrium Morphology Development in Seeded Emulsion Polymerization. IV. Influence of Chain Transfer Agent

Jeffrey M. Stubb, Donald C. Sundberg

Polymer Research Group, Nanostructured Polymers Research Center, Materials Science Program, University of New Hampshire, Durham, New Hampshire 03824

Received 15 March 2005; accepted 1 November 2005
DOI 10.1002/app.23643
Published online in Wiley InterScience (www.interscience.wiley.com).

ABSTRACT: We performed a series of experiments to study the effect of a chain transfer agent, *n*-dodecyl mercaptan (*n*-DM), on the development of morphology in composite latex particles. The morphologies were determined using a combination of transmission electron microscopy, differential scanning calorimetry, and surfactant titration. The polymer molecular weights were reduced up to 10-fold with *n*-DM levels up to 1.4% in the monomer. The addition of *n*-DM can increase the extent to which second-stage polymer domains are formed within the interior regions of the seed particles, but this is only expected under specific conditions. Numerical simulations support this conclusion. We also observed that the reduction in the molecular weight of the second-stage polymer did not significantly increase the extent of phase separation and morphology rearrangement within the particles. The overall effect on the morphology was limited. © 2006 Wiley Periodicals, Inc. J Appl Polym Sci 102: 945–957, 2006

Key words: nanocomposites; core–shell polymers; emulsion polymerization; molecular weight distribution; molar; morphology

INTRODUCTION

The use of composite latices having particles containing two or more thermoplastic polymer phases is extensive throughout the coatings, adhesives, and impact modifier industries. These composite latices are produced by starting with a "seed" latex of one type of polymer and polymerizing a second monomer within the existing seed particles during a second-stage process. Most polymers are incompatible, so the polymers phase separate during the polymerization. The properties of the obtained products strongly depend on the phase separated structure, or morphology, within the particles themselves. The most stable morphology is determined by thermodynamics and represents a state where the interfacial energies within the system are minimized.[1–5]

More often than not, this equilibrium morphology is not achieved; but the morphology is instead determined by the complex interplay between the simultaneous processes of reaction and diffusion within the particles. Such morphologies are formed under kinetic control and are thus nonequilibrium type structures. It has become abundantly clear that the rate at which second-stage polymer radicals diffuse into the particles after entry from the aqueous phase (we termed this radical penetration) is a major controlling factor.[6–8] The idea of limited radical penetration has also been supported by the independent work of several other researchers, mostly through the use of mathematical modeling.[9–13] A second important factor is the process of polymerization induced phase separation of the seed and second-stage polymers within the particles during the polymerization.[14,15] Recently, we have investigated several factors that influence the development of nonequilibrium morphologies including the influence of the seed polymer glass-transition temperature (T_g) and reaction temperature,[7] initiator types,[8] and mode of monomer addition.[6,7] This body of work has shown that the T_g of the polymers, especially of the seed polymer in relation to the reaction temperature, is of major importance. The type of initiator (ionic vs. nonionic) as it relates to the possible anchoring of second-stage polymer chains to the particle surface is of much less importance, and it only has an effect over a relatively narrow range of conditions.

The present communication describes a study aimed at determining the effect that a chain transfer agent (CTA) added during the second-stage polymerization has on the development of nonequilibrium latex particle morphologies. To the best of our knowledge, no study has ever been conducted to specifically investigate this issue. However, many researchers

Correspondence to: J. M. Stubb (jstubbs@cisunix.unh.edu).
Contract grant sponsor: UNH Latex Morphology Industrial Consortium.

have investigated the use of CTAs (particularly the mercaptans) in emulsion polymerization in general.[16–26] An important feature of emulsion polymerization systems utilizing mercaptan CTAs is that under some conditions the effectiveness of the CTA may be limited by its mass transfer from the monomer droplet, through the water phase, and into the polymer particle where it is needed to control the molecular weight distribution (MWD). The significance of this mass transfer limitation has been known since at least the 1960s,[16] but Nomura et al. were the first to model this quantitatively.[17] This is a complicated subject that we will return to later.

Mechanistic considerations

Previous modeling[6–13] and experiments[6–8] have shown that a major factor impacting nonequilibrium morphology development is the diffusion rate of second-stage polymer radicals within the seed particles during the polymerization. The majority of the distance that the radicals penetrate into particles is determined by the distance they can diffuse soon after entry, while they are still relatively short oligomers.[6,8] This is not surprising given that the diffusion rate coefficient of polymer chains (or oligomeric radicals) decreases with the inverse square of the chain length (i; $D \propto 1/i^2$).[27] When a polymer radical chain transfer reaction occurs, either to the monomer or to the CTA, a small radical (a unimer) is produced that can then diffuse much more rapidly than its parent radical (which likely contained 100s or 1000s of monomer units in the chain). It is expected that increasing the frequency of chain transfer reactions will greatly enhance the ability of second-stage radicals to penetrate the seed particles, and thus is likely to affect the particle morphology. This is the motivating factor behind studying the effect of CTAs on nonequilibrium morphology development.

We chose to work with systems having seed polymer T_g values in the range of 50°C with a reaction temperature of 70°C. Such systems provide the greatest ability to observe the effect of CTAs because previous work[6–8] has shown that in such cases polymer radicals are able to penetrate to a significant extent, but not completely, giving rise to "occluded core–shell" (CS) type morphologies. (We used the term occluded CS previously[6–8] to describe morphologies in which the second-stage polymer is present as many separate domains dispersed within the seed polymer matrix, with the domains being preferentially located in the shell region.) In systems where penetration is either extremely limited (T_g of seed $\gg$ reaction temperature) or full penetration is assured (T_g of seed $\ll$ reaction temperature), it is likely to be difficult to observe a CTA effect on the morphology if one does in fact exist.

The use of CTAs creates shorter dead polymer chains and produces new, very short radicals. Thus, changes in morphology will potentially be impacted by both factors, with the short radicals promoting radical penetration and the lower molecular weight polymer promoting phase separation and rearrangement. To separate the two effects, two different systems were designed in this work, one having an inverted CS (ICS) equilibrium morphology and the other having a CS equilibrium morphology. For convenience, we refer to these as the CS and ICS systems throughout this article. This convention should not be confused with an assumption that these equilibrium morphologies will actually be formed experimentally. (In fact, we expect that they will not.) For the ICS system both effects will serve to increase the likelihood of finding a second-stage polymer in the interior of the final composite particles. However, for the CS system, significant radical penetration will increase the likelihood of finding a second-stage polymer in the particle interior, whereas significant dead polymer diffusion will increase the likelihood of finding it in the outer shell. Computational verification of the ICS and CS equilibrium morphologies for the systems we chose to study was obtained by modeling with UNHLATEX™ EQMORPH software.[5]

In-depth kinetic modeling was also performed using UNHLATEX™ KMORPH software[28,29] to help explain any observed effects of increased radical penetration on morphology development. KMORPH considers the development of morphology in a dynamic sense by quantifying the extent of radical penetration. Whereas previous publications[28,29] describe the details of the models and the mathematical relationships used in the program, the consideration of chain transfer to CTAs was not considered at the time of their publication. Since then, we have extended the models to account for CTAs by including a new differential equation to calculate the CTA concentration and modifying the differential equations for the radical concentrations. The equation describing the CTA concentration is the following:

$$\frac{d[\mathrm{CTA}]}{dt} = \frac{m_{\mathrm{feed}} w_{\mathrm{cl}} MW_{\mathrm{CTA}}}{V_p} - C_{\mathrm{cf}} k_p [\mathrm{CTA}][R^p_{\mathrm{tot}}] \quad (1)$$

where [CTA] is the concentration of CTA in the polymer phase, $[R^p{}_{\mathrm{tot}}]$ is the total radical concentration in the polymer phase, m_{feed} is the mass feed rate of monomer to the reactor, w_{ct} is the weight fraction of CTA in the monomer, $\mathrm{MW}_{\mathrm{CTA}}$ is the molecular weight of the CTA, V_p is the volume of the polymer phase, and C_{ct} is the ratio of the chain transer coefficient for CTA ($k_{\mathrm{tr,CTA}}$) divided by the propagation rate coefficient (k_p). Here, it is clear that we have not considered any mass transport difficulties of the CTA in moving

TABLE I
Recipes for Pre-Seed Latices

System	ICS	CS
Monomer 1 (g)	MMA; 44.50	BA; 27.64
Monomer 2 (g)	MA; 44.65	St; 61.43
Monomer ratio, wt 1 : wt 2	50MMA : 50MA	31BA : 69St
Water (g)	800.22	800.46
SDS (g)	2.00	2.03
$NaHCO_3$ (g)	0.50	0.50
KPS (g)	0.65	0.65
Measured solids (wt%)	10.10	10.18
Measured diameter (nm)	72	75

from the emulsified droplets of monomer to the water phase and into the latex particles. Our approach to account for this is described in Appendix A. The differential equation for the concentration of radicals of length i is

$$\frac{d[R_i^p]}{dt} = k^*_p[M^p]\{[R_{i-1}^p] - [R_i^p]\} - k_{tr,M}[M^p][R_i^p] - k_{tr,CTA}[CTA^p][R_i^p] - k_{i,j}[R_i^p][R_{tot}^p] \quad (2)$$

where $[R_i^p]$ is the concentration of radicals having i number of repeat units, $[M_m^p]$ is the monomer concentration in the polymer phase, and $k_{tr,M}$ is the rate coefficient for chain transfer to the monomer. This is the same equation as previously described,[29] including chain transfer to the monomer, except that the term describing the chain transfer to the CTA has been inserted.

We find that a useful concept is the number of transfer events experienced per radical that entered the particle from the aqueous phase. This is given by the following equation:

$$\text{transfers/entered radical} = \frac{k_p(C_M[M_p] + C_{CT}[CTA])}{\langle k_i \rangle [R_{tot}^p]} \quad (3)$$

where C_M is of the rate coefficient for chain transfer to the monomer divided by k_p and $\langle kt \rangle$ is the overall or apparent termination rate coefficient. In the Results and Discussion Section we will refer to this ratio in the context of analyzing the experimental morphology data.

EXPERIMENTAL

Our goal in the experimental portion of this work was to produce two latex systems designed to enhance the opportunity to observe the effect of chain transfer events on particle morphology, with each system offering a different environment in which to judge the results. The first system used a seed polymer of poly(methyl acrylate-*co*-methyl methacrylate) [P(MA-*co*-MMA)] with styrene (St) as the second-stage monomer, representing an ICS system. The second system used a seed polymer of poly(butyl acrylate-*co*-St) [P(BA-*co*-St)] with MMA as the second-stage monomer, representing a CS system. The MWDs of the resulting second-stage polymers were determined using gel permeation chromatography (GPC) and the morphologies of the composite particles were characterized using transmission electron microscopy (TEM), differential scanning calorimetry (DSC),[15,30–33] and surfactant titration.[34–37]

Seed latex preparation and characterization

The seed latices were produced by growing the particles slowly in a semibatch, starve-fed manner (1-L reactor, Teflon impeller, 70°C) in order to eliminate compositional drift in the copolymerization. In each case the seed polymerizations utilized a "preseed" latex, which allowed control over the final particle size. The preseed latices were produced using the same comonomer ratios as in the growth stages of the seed latex, but in a batch manner to produce particles significantly smaller than that desired for the final seed latex particles. The recipes are given for the preseed polymerizations in Table I and for the seed latices in Table II. The monomers were fed to the reactor over a total time of 6 h using 50-mL glass syringes driven by syringe pumps. The final particle sizes obtained for the seed latices were 182 nm for the ICS system and

TABLE II
Recipe for Growth of Seed Latices

System	ICS	CS
Preseed latex (g)	84.92	84.95
Water (g)	666.81	666.82
$NaHCO_3$ (g)	0.49	0.49
SDS, initial charge (g)	0.20	0.20
KPS, initial charge (g)	0.17	0.17
Monomer 1	MMA	BA
Monomer 2	MA	St
Monomer ratio, wt 1 : wt 2	50MMA : 50MA	31BA : 69St
Monomer feed rate (g/hr)	31.53	31.53
Monomer feed time (hr)	6	6
Total monomer fed (g)	189.2	189.2
KPS, late charge (g KPS : g water : time (min))	0.05 : 10.12 : 182	0.05 : 10.02 : 183
SDS, late charges (g SDS : g water : time (min))		
1	0.13 : 25.13 : 150	0.13 : 26.07 : 150
2	0.08 : 25.00 : 302	0.08 : 24.85 : 301
Measured solid content (wt%)	17.57	17.60
Measured diameter (nm)	188	195

TABLE III
Recipes for Second-Stage Polymerizations

System	ICS	CS
Seed latex (g)	79.7	75.6
Water (g)	116.6	117.0
$NaHCO_3$ (g)	0.05	0.05
SDS (g)	0.07	0.10
KPS (0.01M solution)		
Initial charge (g sol'n)	3.8	3.4
Feed rate (ml/hr)	0.8	0.8
total KPS sol'n fed (g)	2.8	2.8
Monomer type	Styrene	MMA
Monomer feed rate (g/hr)	7	7
Total monomer fed (g)	14	14
n-DM concentrations used (wt% in monomer)	0; 0.11; 0.25; 0.59; 1.25	0; 0.15; 0.60; 1.40

186 nm for the CS system as measured by capillary hydrodynamic fractionation (CHDF). The T_g values of the dry polymers, measured by DSC, were 51°C for system ICS and 53°C for system CS; and the transitions were fairly narrow (approximately 20°C), indicating that compositional drift during the copolymerization was minimal.

Second-stage polymerizations

In all cases, the monomer was fed to the reactor over a period of 2 h. Potassium persulfate (KPS) initiator solution was added in the form of a 0.01*M* solution, and it was also fed to the reactor throughout the polymerization at a rate equal to the rate that the initiator was being consumed (calculated using a dissociation rate coefficient for KPS[38] of 2×10^{-5} s^{-1}) in order to maintain a constant rate of radical production throughout the polymerization. The recipe used for all second-stage polymerizations is given in Table III. *n*-Dodecyl mercaptan (*n*-DM) was added directly to the monomer before it was fed to the reactor, and the concentrations were varied up to 1.4 wt % (see Table III).

Chemicals

St, MA, MMA, and BA monomers (Acros Organics) were passed through a column of alumina adsorption powder (80–200 mesh, Fisher Scientific, Fairlawn, NJ) to remove inhibitors and stored at −10°C prior to use. Analytical grade KPS (Acros Organics), analytical grade sodium bicarbonate (EM Science), sodium dodecyl sulfate (SDS, 99%, Acros Organics), and *n*-DM (Acros Organics) were used as received. Deionized water from a Corning Mega Pure D2 water purification system was used in all experiments.

Analytical methods

In order to confidently determine the morphology of the composite latex particles, it is usually necessary to utilize a number of independent, complimentary analytical techniques,[36] each of which may provide a somewhat different piece of information.

Particle size

The particle sizes of all latices were measured using a CHDF 2000 from Matec Applied Sciences. The instrument was calibrated over a range of 30–700 nm using particle size standards [polystyrene (PS) latices] obtained from Seradyn Inc.

GPC

The MWDs of the second-stage polymers were determined using GPC with a system comprising Waters components and equipped with both refractive index (RI) and UV detectors. A bank of four columns were arranged in series (three Styragel HMW 6E columns and one HMW 7) and calibrated with PS standards obtained from Polysciences Inc. For the ICS system, the MWD of the second-stage polymer (PS) was obtained directly from the response of the UV detector, because the P(MA-*co*-MMA) seed polymer does not absorb UV light at the wavelength of the detector (254 nm). For the CS system, the RI detector response was utilized and the RI peak of the neat seed latex (injected separately) was subtracted from that of the composite latices to obtain the MWD of the second-stage polymer alone. (The magnitudes of the RI signal were first normalized to reflect the ratio of the different polymers in the mixed vs. straight solutions.) This peak subtraction procedure was tested using separate solutions and a mixed solution of very high molecular weight PS and poly(MMA) (PMMA). The weight-average molecular weight (M_w) of the PMMA polymer determined from its individual injection was 1,939,100 g/mol and that determined by the subtraction procedure was 2,025,600 g/mol, reflecting a difference of less than 5%. This test confirmed that the subtraction procedure is sufficient to obtain a reasonable measurement of the MWD of the second-stage PMMA for the CS system. It should be noted that the PMMA molecular weights were not corrected to account for the fact that the GPC was calibrated using PS standards. Performing such a correction, for instance, based on Mark–Houwink–Sakurada coefficients from the literature,[39] would result in a correction of about 25% for the PMMA molecular weights reported here. Because this correction applies to experiments with and without CTA, it does not affect our calculations for the number of transfer events per entered radical and therefore has no influence on the conclusions developed in this work.

DSC

DSC was performed using a Pyris 1 power compensated DSC apparatus from PerkinElmer.[40] This was

TABLE IV
Particle Sizes and Molecular Weights of Seed and Second-Stage Polymers

Experiment	Particle Diameter (nm)	Weight Average MW (M_w, g/mol)	Polydispersity, M_w/M_n
System A			
Seed latex	182	Not available	
0 % n-DM	231	910,600	2.8
0.11% n-DM	230	480,300	3.7
0.25% n-DM	234	365,900	3.6
0.59% n-DM	231	273,000	3.3
1.25% n-DM	233	155,700	4.3
System B			
Seed latex	186	1,216,900	5.4
0% n-DM	223	1,537,000	4.5
0.15% n-DM	223	439,000	3.4
0.60% n-DM	223	233,000	3.5
1.40% n-DM	225	121,000	4.8

used to determine the T_g values of the seed polymers and to observe the range over which the transition occurred. Relatively narrow glass-transition ranges were taken as evidence that compositional drift was not significant during the copolymerizations to grow the seed latices. The step-scan DSC technique (creates effects similar to temperature modulation) was used to study the extent of mixing of the polymers in the composite particles formed during the second-stage polymerizations. The process of using DSC to study the phase separated characteristics of composite latex particles has been described in detail in a separate publication.[15] The technique has also been applied by other researchers on various polymer blends and composites.[30–33]

Surfactant titrations

Surfactant titrations were utilized to determine the extent to which the surface of the composite particles is covered by the seed and/or second-stage polymers. This technique has been described in detail elsewhere.[34–37] It takes advantage of the fact that different polymer surfaces adsorb different amounts of the same surfactant, with polar surfaces adsorbing less surfactant than the nonpolar surfaces. The fractional coverage of the two polymers on the surface of the composite particles is calculated using eq. (4), where A_s is the adsorption area of the surfactant on the composite particles; A_{s1} and A_{s2} are the adsorption areas on the seed and second-stage polymers, respectively; and f_2 is the fraction of the composite particle surface that is covered by the second-stage polymer:

$$f_2 = \frac{1/A_s - 1/A_{s1}}{1/A_{s2} - 1/A_{s1}} \quad (4)$$

TEM

The sample preparation techniques used for TEM analysis were described previously.[36] Samples of the final latices were dried at room temperature to remove water and then ground into a powder. A small amount of the powder was then embedded in a two-part epoxy and cured overnight at room temperature. Microtomed sections of approximately 60–90 nm thickness were observed in a Hitachi H600 transmission electron microscope. The particles were stained with ruthenium oxide vapor for 5–10 min before viewing in the TEM apparatus to improve the contrast between the St containing phase (dark) and the all acrylic phase (light).

RESULTS AND DISCUSSION

The final particle sizes of all seed and second-stage latices are given in Table IV. The CHDF analysis (95% accuracy) confirmed that new particle formation did not occur during the second stage because only a single narrow peak was detected in the chromatograms and, according to our experience, new particles (if formed) are significantly smaller than the seed particles used in these experiments. In addition, the volume ratio for the final composite particles compared to the seed particles agreed with the extent of particle growth expected from the stage ratio and polymer densities. This further confirms that new particle formation did not occur. Samples withdrawn during the second-stage polymerization were analyzed by gravimetric analysis to confirm the starve-fed nature of the reactions. Figure 1 shows the conversion versus time for the control experiments from both the ICS and the CS systems in which a CTA was not used. It is clear that the overall fractional conversion of monomer to polymer line lies essentially parallel to that representing the fraction of the total monomer that had been fed, a characteristic of a starve-fed polymerization.

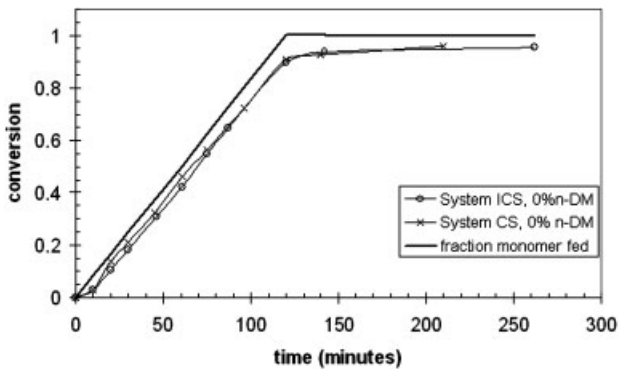

Figure 1 Examples of conversion versus time profiles for two polymerizations with 0% *n*-DM for both systems. The data are characteristic of all other experiments.

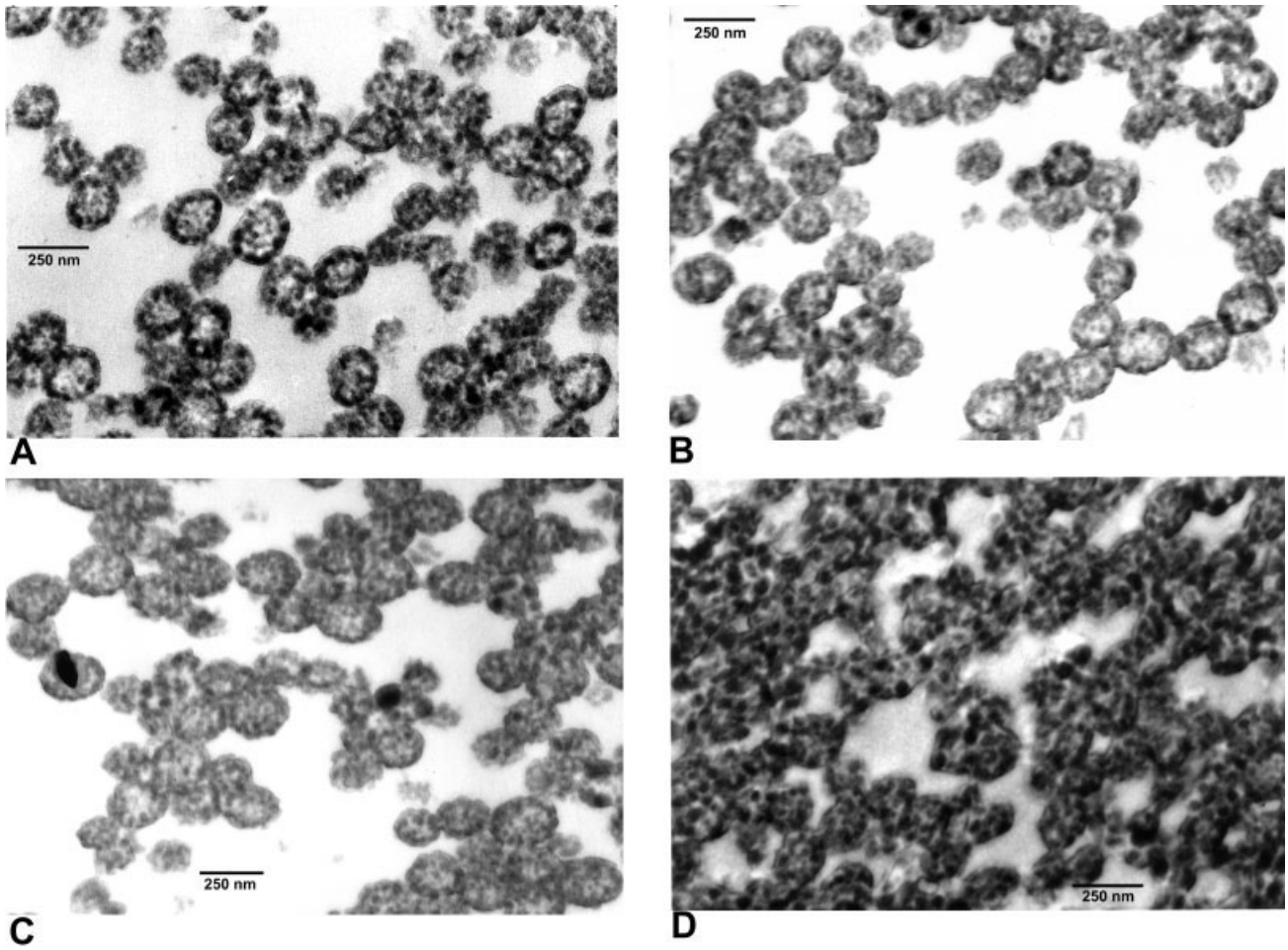

Figure 2 TEM photos of microtomed sections of the composite particles produced in the ICS system polymerizations with (A) 0, (B) 0.11, (C) 0.59, and (D) 1.25% *n*-DM.

The results for all other experiments were essentially the same as in Figure 1 and are not included here for the sake of brevity.

GPC analysis of the composite latices showed that the MWDs were monomodal for all second-stage experiments. Table IV provides the M_w values and polydispersity indexes (M_w/M_n) for the seed polymers and all second-stage experiments. The M_w decreased by almost a factor of 10 when moving from the experiments with no CTA to those with the highest concentration of *n*-DM whereas the M_w/M_n remained about the same, ranging from 3 to 4. Therefore, there was a large difference in the frequency at which small radicals were formed within the particles when comparing the experiments with different *n*-DM concentrations. In addition, because the diffusion coefficient of polymer chains changes as i^{-2}, the dead polymer chains produced with the highest *n*-DM concentration will be able to move and rearrange 100 times faster in the particles compared to those produced without any added CTA.

The second-stage polymer molecular weights produced for the experiments in the ICS and CS systems are very similar when compared at equal *n*-DM concentrations. Thus, *n*-DM was equally effective at lowering the molecular weight of both monomers used in the second-stage experiments. This is despite the fact that the C_{ct} is larger by about a factor of 5 in the St system (ICS) compared to the MMA system (CS).[39] This result is due to the semibatch, starve-fed nature of the polymerizations, which allows the process to reach a steady state and prevents the *n*-DM from being consumed preferentially compared to the monomer.

Morphology analysis for ICS system

The TEM results are providedd in Figure 2. In all cases the particles display occluded-type morphologies, in which the PS phase exists as many separate domains within the particles. This suggests that the diffusion of the dead polymer chains was not possible or was fairly slow during the polymerization, so that the microdomains did not have a chance to rearrange and consolidate even though the domains are quite close together. It is favorable from a thermodynamic stand-

TABLE V
Surfactant Titration Results for System ICS

Latex	A_s (Å^2/molecule)	% of surface covered by 2nd stage polymer
P(MA-co-MMA) (seed)	134	N/A
0% n-DM composite	93	21
0.11% n-DM composite	102	14
0.25% n-DM composite	104	13
0.59% n-DM composite	97	18
1.25% n-DM composite	138	0
Polystyrene (2nd stage)	43	N/A

point to combine several domains into one, thus leading to decreased interfacial area between the seed and second-stage polymer phases (i.e., to undergo Ostwald ripening). Therefore, consolidation would have occurred if significant polymer diffusion had been possible.

In terms of the present work, a major feature is the degree of penetration of the second-stage PS into the center of the particles. It is clear that all of the experiments did result in some amount of the PS phase in the interior regions of the particles, even when no CTA was used. If one compares the lowest and highest concentrations of CTA, 0% in Figure 2(A) and 1.25% in Figure 2(D), it is very clear that the PS phase in Figure 2(A) is preferentially located within the outside shell region of the particles and in Figure 2(D) it appears to be distributed evenly throughout the particles. This suggests that increased levels of CTA did in fact increase the extent of penetration of the second-stage polymer into the seed particles. When one also considers the photos in Figure 2(B,C) in order to observe a continuous trend of increasing CTA concentration, it appears that as the CTA concentration is increased the degree of penetration continuously increases. However, the differences between each successive experiment are rather subtle. It is also clear that the domains in Figure 2(D) are larger than in Figure 2(A), suggesting that increased CTA levels promoted some limited extent of polymer rearrangement after the chains phase separated and/or terminated. This is consistent with having faster rates of polymer diffusion at lower polymer molecular weights.

The results of the SDS titrations for the ICS system are shown in Table V. The adsorption areas represent the average value obtained for at least two, but often three, separate titrations. As expected, the A_s for the pure second-stage PS (42.5 Å^2/molecule) is much lower than the value of 133.5 Å^2/molecule for the P(MA-*co*-MMA) seed polymer. The values for the composite particles are in between the seed and second-stage polymers, except for the experiment with the highest *n*-DM concentration that is just slightly above the seed polymer A_s value. Using eq. (4), the fraction of the surface that is covered by the second-stage polymer was calculated and the values are given in Table V. The results show that at all CTA concentrations the surface is dominated by the seed polymer. This may seem surprising given the TEM results discussed earlier. However, the surfactant titrations are only sensitive to the extreme surface of the particles and because the PS is present in separated domains with the seed polymer being the continuous phase within the particles, it is actually not surprising that the seed polymer covers the majority of the surface. This behavior is favored from a thermodynamic perspective, because the seed polymer/water interfacial tension is much lower than that between the second-stage PS and water.[41] The most interesting result from the titrations is observed for the experiment with 1.25% *n*-DM. In this case, the surface is apparently covered entirely by seed polymer. This suggests that the second-stage polymer was able to remove itself from the surface more easily than in the other experiments, exposing the seed polymer to the water phase to a greater degree. The larger domain sizes suggest that PS achieved some degree of reconfiguration after the initial phase separation and may have moved away from the surface of the particle. This result is also consistent with increased radical penetration.

The DSC results for this system are shown in Figure 3. The data are plotted in derivative form so that the glass transitions appear as peaks, which aids in the interpretation of the data. These results provide us with information about the degree of phase separation (on a molecular scale) between the two polymers within the composite particles.

The DSC traces for the pure seed and second-stage polymers are included in Figure 3 for reference. The maximum values of pure polymer transitions are larger than for the transitions in the composite because all of the polymer in the pure samples experiences the glass transition in the same temperature range. In the

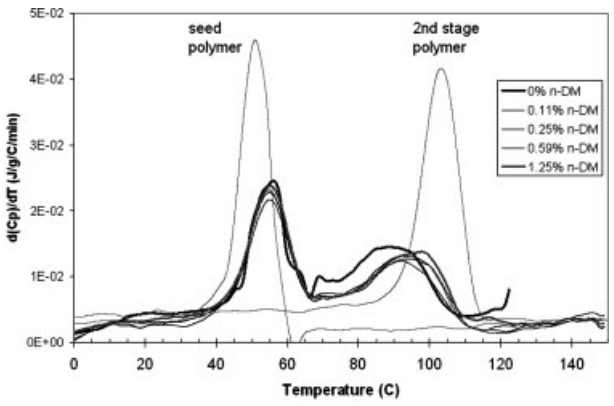

Figure 3 Step-scan DSC results for the composite particles produced in the ICS system polymerizations.

composites, the total material is divided into multiple transitions so each transition appears smaller. In Figure 3, the data for all of the composites are similar, with each experiment exhibiting two distinct glass-transition peaks. The results in the figure for the 0 and 1.25% *n*-DM experiments are indicated by thick lines. All other experiments are indicated by thin lines and are not differentiated from one another because they are essentially identical. The first feature to note in Figure 3 is that the glass-transition peak for the seed polymer in the composites moved to a higher value compared to the pure seed polymer and that for the second-stage polymer has moved to a lower value. It is also observed that the data do not return to baseline in between the two T_g peaks. Both features indicate that there is a substantial degree of mixing between the two polymers and a large amount of interfacial material present, which is characteristic of systems that have not been able to phase separate to an equilibrium state during the polymerization (not to be confused with achieving an equilibrium morphology, which requires further rearrangement after phase separation has occurred). This agrees well with the occluded-type morphologies observed in the TEM images in which the domain sizes were very small. It is also interesting to note that the second-stage T_g peak for the experiment with 0% *n*-DM moved to lower temperatures by the largest amount out of all the experiments, and the data for this experiment remain substantially above the baseline values in between the pure polymer T_g values. This suggests that this experiment has the lowest degree of polymer phase separation of all the experiments. Another interesting feature is that, even for the experiment with 1.25% *n*-DM, a large amount of interfacial material and a significant degree of mixing remains. Therefore, even when the average molecular weight of the dead polymer is reduced by a factor of 6 compared to the experiment with no CTA, polymer diffusion is still very restricted and limits rearrangement within the particles. The TEM for the 1.25% *n*-DM experiment [Fig. 2(D)] did show larger domains, which suggests more phase separation and less interfacial material; but this difference is not reflected in the DSC data when compared to those for lower CTA levels.

Morphology analysis for CS system

The TEM photos for the CS system are shown in Figure 4(A–D). The most striking characteristic is that the particles do not display any obvious structural features, such as those observed for the former system. Many particles appear lighter than others. These represent particles that were not sectioned through the center, and thus should be mostly disregarded. The larger particles, which are the darkest, seem to indicate a thin outer shell of lighter material, which could be interpreted as being some of the second-stage PMMA.

For the ICS system, it was possible to observe domains of second-stage material within the interior of the particles and to make judgments about the varying degrees of penetration between the different experiments. In Figure 4, there are no apparent internal domains of second-stage PMMA within the particles. There are two possible reasons for this. The first is that they simply are not present. The second is that it is not possible to observe small domains of the lighter (unstained) PMMA phase contained within a continuous phase of the darker (stained) P(BA-*co*-St) seed polymer. Given that there are no observable differences between the TEM results for these experiments, it is not possible to draw direct conclusions about the effect of the CTA for this system with only these data.

The results of the surfactant titrations are provided in Table VI. The adsorption areas on the composite particles are much closer to that of the second-stage PMMA than that of the P(BA-*co*-St) seed polymer. In fact, calculations via eq. (4) show that the particle surface is covered by 88–100% second-stage polymer. This supports the notion that the particles possess a thin outer layer of PMMA, as may be indicated by the TEM photos. However, the surfactant titrations do not provide any information about how thick this PMMA layer may be.

The DSC results for the CS system are shown in Figure 5. It quickly becomes clear that the characteristics of this system are very different from the ICS system. Here, only one glass-transition peak is observed for all of the experiments, and this peak is located entirely in between the glass-transition peaks for the pure seed and second-stage polymers. The data for all four experiments are very similar to one another in this sense. This result means that there was essentially no phase separation between the two polymers for any of these experiments, and the seed and second-stage polymers are mixed in what can be considered an unstable solid solution within the particles. This result, although somewhat surprising, actually helps one to understand the TEM photos in Figure 4. The reason that the particles do not exhibit any obvious structural features is because there is only one, mixed polymer phase present within them. When carefully examining the DSC data in Figure 5, there appears to be an indication of a small peak, or an extended shoulder, in the range of 110°C. This is close to the T_g of PMMA (about 120°C) and indicates a very small amount of material that is rich in PMMA does exist within the particles. In this case, it is likely that this PMMA-rich material is actually present as a shell around the particles, a conclusion that is supported by the surfactant titration results in Table VI.

Although the results for this CS system do not show any clear differences or trends between the experi-

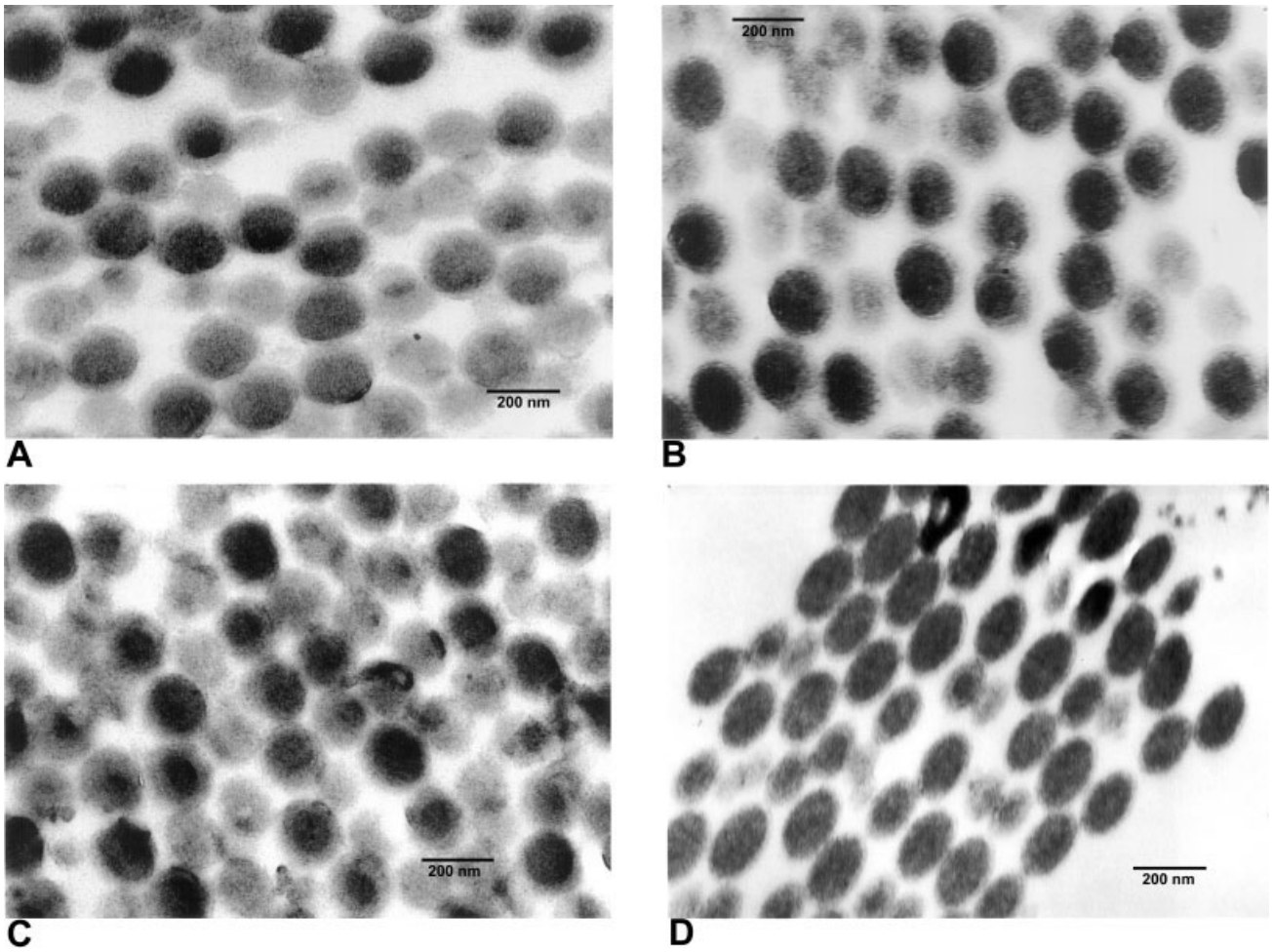

Figure 4 TEM photos of microtomed sections of the composite particles produced in the CS system polymerizations with (A) 0, (B) 0.15, (C) 0.60, and (D) 1.40% *n*-DM.

ments, it is still possible to gain some understanding about the effect of the CTA in this system. Given that even the experiment with no CTA did not show any obvious structural features and produced a particle with only one broad T_g, it can be said that the radicals are able to fully penetrate into the interior of the particles even without added CTA. This must be true because otherwise there would be an internal region composed predominantly of seed polymer, which would be observable as a separate peak in the DSC (even if it was not clearly visible in the TEM). This result is consistent with the results for the ICS system, in which a significant number of domains of second-stage PS were observed in the particle interior even in

TABLE VI
Surfactant Titration Results for Systems CS

Latex	A_s (Å^2/molecule)	% of surface covered by P2
P(BA-co-St) (seed)	46	N/A
0% n-DM composite	141	100
0.15% n-DM composite	101	88
0.60% n-DM composite	112	95
1.40% n-DM composite	116	98
PMMA (2nd stage)	120	N/A

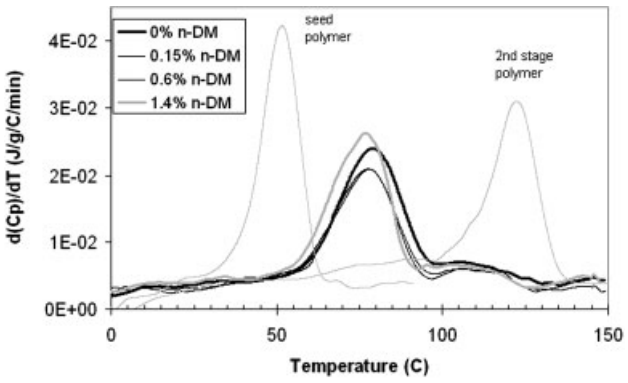

Figure 5 Step-scan DSC results for the composite particles produced in the CS system polymerizations.

the experiment without CTA. Although it is not possible to observe differences in the extent of penetration in this system as it was for the former system, the major reason for including this system here was to observe whether increased dead polymer diffusion due to lower polymer molecular weights allowed for more rearrangement toward the equilibrium morphology (CS). In this case, it is clear that even when the molecular weight was reduced by a factor of 10 using CTA, diffusion of the dead polymer was still extremely limited, so much so that the chains could not even phase separate from the seed polymer. If chains are not mobile enough to phase separate, then rearrangement of the morphology, which requires diffusion over larger length scales, will not be a factor and will not be impacted as CTA is added. The reason that the extent of phase separation was less than for the ICS system is likely that the T_g of the PMMA in the CS system is about 15–20°C higher than for the PS in the ICS system.

Computer simulations

In order to help understand the mechanisms responsible for the changes in morphology observed in the experiments, simulations were performed using the UNHLATEX KMORPH software package,[28,29] as noted earlier. Here, the development of morphology is considered from a kinetically controlled perspective by modeling the diffusion of polymer radicals within the particle. Chain length dependent termination reactions are thoroughly accounted for. The critically important diffusion coefficients are calculated as described in the literature.[42] The morphology prediction is reached by tabulating the radial position within the particle where each polymer radical was terminated throughout the entire polymerization. This results in a spatial distribution describing where the second-stage polymer was formed within the particle, and it can be used to construct a simulated TEM image. Areas of seed or second-stage polymer can be colored different levels of gray to simulate different staining levels of the two polymers and a graphical representation can be displayed.

To make the simulations useful in this study, it was necessary to address the level of agreement between the predicted and experimental molecular weights for different levels of CTA. It was first necessary to adequately predict the polymer chain length with no CTA, while still accounting for chain transfer to the monomer (chain transfer to the polymer has not yet been introduced to the model). Good agreement was obtained at the zero CTA level (Table VII) by allowing all of the oligomeric radicals in the water phase to enter the particles. This is not as we would like it because radical entry efficiencies are often reported to be less than 100%, especially for St monomer.[38] However, it suits the purpose of this particular study by providing a suitable base case for all simulations, and it works well for both St and MMA. All remaining simulations utilized the same water phase termination parameters.

TABLE VII
Summarized MW Results from KMORPH Simulations

Experiment	MW_w (experiment)	MW_w (KMORPH)	Transfers per entered radical
System ICS			
0% n-DM	910,600	940,000	0.3
0.11%	480,300	520,000	1.4
0.25%	365,900	380,000	2.5
0.59%	273,000	265,000	4.1
1.25%	155,700	190,000	5.4
System CS			
0% n-DM	1,537,000	1,500,000	0.2
0.15%	439,000	500,000	2.7
0.60%	233,000	230,000	7.0
1.40%	121,000	138,000	12.0

One further and important adjustment was necessary in order to accurately predict the molecular weights formed in the experiments using *n*-DM. It is well known that the mass transfer of *n*-DM across the emulsified droplet interface and/or through the water phase is often a limiting step in emulsion polymerization.[16–25] This results in *n*-DM being less effective for altering the molecular weight than it would be in a bulk or solution polymerization. Previous studies[25] have shown that this effect can be handled by assigning an "effective" chain transfer coefficient for each monomer and using it rather than the coefficients reported from bulk or solution polymerization systems with the same monomer. The details of such adjustments for the monomers used in the present study are described in Appendix A. The result for our study was that the normal chain transfer coefficient for St was adjusted by a factor of 0.007 and that for the MMA by 0.02, irrespective of the level of *n*-DM used in the experiment. The simulated and experimental molecular weight results for all of our experiments can be compared by referring to Table VII. Agreement is exceptional, considering that the resultant molecular weights were decreased by a factor of 10 upon the use of slightly more than 1% *n*-DM based on the monomer. Other than the two adjustments described above, no other adjustable parameters were utilized in the simulation.

From a morphological perspective, as the number of chain transfer events resulting from each radical entering from the water phase increases with increasing levels of CTA, the likelihood of polymer radicals diffusing to the center of the particle should increase. This would lead to more penetration of the second-stage polymer within the seed latex particle. Even

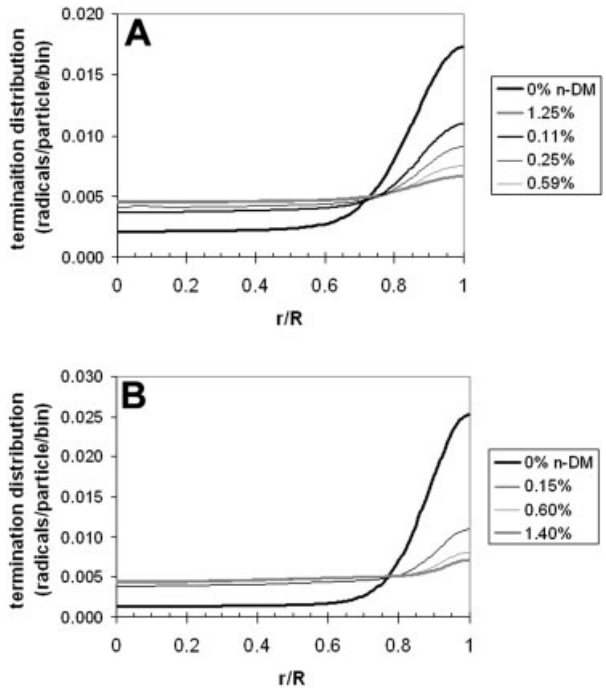

Figure 6 The radial distribution of termination events within the particles from simulations with UNHLATEX KMORPH.

without CTA, some transfer reactions occur because of chain transfer to the monomer, which is always a possibility in emulsion polymerization. Table VII shows the computed number of chain transfer events for each entering oligomeric radical and the significant increases created by using higher levels of *n*-DM.

Figure 6(A) shows the radial distributions of the termination events within the particles for the simulations of all experiments for the ICS system. Even for the experiment with 0% *n*-DM, some second-stage polymer was expected to be formed in the center of the particles, because the radial distribution levels out in the interior region of the particle. This is due to radicals that underwent transfer (to monomer in this case) and produced new, short radicals that are able to continue diffusing toward the center of the particle. As the concentration of CTA increases, the distributions continuously favor more second-stage polymer formed in the interior of the particles, with less likelihood of it preferentially forming in the outer region. By the time the highest CTA concentration is reached, the distribution suggests that the polymer is formed rather uniformly throughout the particle. Figure 7(A) shows the TEM simulations based on the radial distributions in Figure 6(A) for the experiments in the ICS system with 0 and 1.25% CTA. It is clear that the simulations resemble the actual TEM images in Figure 2 quite closely, except that the domain sizes in Figure 2(D) are much larger than in Figure 7(A) for the 1.25% *n*-DM level. It appears that the low molecular weight second-stage polymer rearranged into larger domains after phase separation [as is evident in Fig. 2(D) compared to Fig. 2(A–C)]. Our simulations do not take Ostwald ripening into account and thus we would not expect to see a match in morphology with respect to domain size. The other experiments also show good agreement between experiment and simulation.

The same type of behavior is predicted for the CS system [Fig. 6(B)] as for the ICS system. These radial distributions suggest that for all experiments, including that with 0% CTA, a significant amount of second-stage polymer should be present throughout the particle, even though the equilibrium structure would have this polymer in a shell. Figure 7(B) shows the simulated TEM photos for the lowest and highest CTA levels used in these experiments. Contrasting these to the experimental results in Figure 4, we have to deal with the fact that our simulations always assume that the second-stage polymer phase separates, whereas in reality it may not. As discussed earlier, the CS system is one in which little or no phase separation took place as clearly seen by the data in Figures 4 and 5. What is consistent between the simulated results in Figures 6(B) and 7(B) and the experimental results is that in all cases the second-stage PMMA is distributed throughout the particle. This must mean that the PMMA radicals reached the center of the particles before terminating.

In general, the results of the simulations are in good agreement with the experimental results, especially for the ICS system where it is possible to visualize the location of the second-stage polymer using TEM. Given that the model assumes a random diffusion process for the polymer radicals, this agreement suggests that after transfer, the new radicals diffuse throughout the particle rather than staying associated with the parent polymer chain.

CONCLUSIONS

In this study we focused on the assessment of chain transfer reactions, both to the monomer and added CTA but not to the polymer, because they may or may not influence the latex particle morphology. We chose to work with a common CTA, *n*-DM, and utilized seed latex polymer T_g values and reaction temperatures such that we knew the second-stage polymer radicals would only partially penetrate the latex particles when no CTA was added. If the seed polymer T_g had been too high, no polymer would have penetrated the seed particle at all and it would not have been possible to observe any effect of the CTA on the morphology. If the T_g had been much lower, all entering oligomeric radicals would have been able to completely penetrate the latex particle and we would not have been able to study the effect of transfer events on penetration. In contrast, we

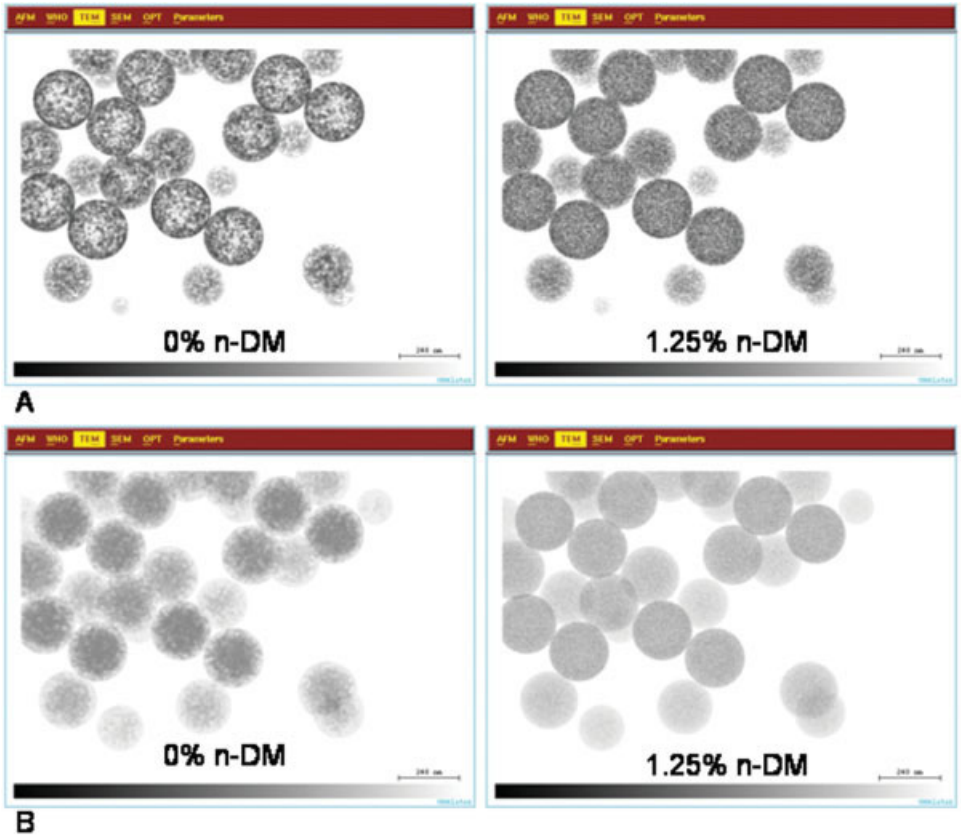

Figure 7 Simulated TEM results from KMORPH simulations for (A) ICS system experiments with 0 and 1.25% *n*-DM and (B) CS system experiments with 0 and 1.4% *n*-DM. [Color figure can be viewed in the online issue, which is available at www.interscience.wiley.com.]

might have been able to study the effect of reduced second-stage polymer molecular weight on the potential of having Ostwald ripening without the complicating features of variable levels of penetration. By using both experimentation and computer simulations we were able to conclude that chain transfer to the monomer and/or CTA leads to morphologies that have enhanced levels of second-stage polymer distributed throughout the latex particle. The more transfer events per entering radical, the higher the probability of enhanced penetration. However, we also concluded that these are not strong effects and we can imagine that in many latex systems they could go unnoticed. Lastly, we point out that chain transfer to the polymer (either seed or second stage) would result in more limited penetration of second-stage polymer radicals because the newly created radical would be high molecular weight and unable to diffuse significantly during the course of the polymerization reaction.

We are grateful for the discussions with our colleagues from the companies in the UNH Latex Morphology Industrial Consortium (Arkema, DSM/NeoResins, Röhm & Haas) and for their financial support of this work.

APPENDIX A

The approach used to model the experiments using UNHLATEX KMORPH[28,29] is explained here. This required an accurate prediction of the kinetics of chain transfer, which is realized by an accurate prediction of the molecular weights observed experimentally. The approach was to first obtain agreement for the experiments without any CTA and then to use the same parameters to model all subsequent experiments. Initially, without any adjustments, the molecular weight predicted by the program was lower than in the experiment. The first approach that we attempted was to adjust the termination rate coefficient (k_t) in the particle phase, which one might expect to decrease the predicted molecular weight. This was unsuccessful because, when k_t is decreased, the concentration of radicals increases, which causes the steady-state monomer concentration to decrease and this tends to lower the molecular weight of the polymer. Therefore, the effect is self-compensating, and the molecular weight could not be effectively altered by simply adjusting the termination rate in the particle phase. The only way to obtain agreement between the predicted and experimental molecular weights for the experi-

ments without CTAs was to decrease the termination rate of radicals *in the water phase*, to the point where all of the radicals that were created entered into particles.

It was also necessary to obtain agreement between the simulated and experimental molecular weights for the experiments with CTAs. When using chain transfer constants (C_{ct}) obtained from the literature[39] (0.55 for *n*-DM/MMA, 2.8 for *n*-DM/St), the predicted molecular weights were drastically less than observed experimentally. In fact, under these conditions the simulations predicted monomer flooded polymerization kinetics because excessive transfer caused excessive termination (through the short–long termination mechanism[26,38]). This does not agree with the monomer starved kinetics observed experimentally, and it is consistent with the fact that CTA mass transfer limitations exist in the experiments but are not accounted for in the simulations. One approach to account for the mass transfer limitations of *n*-DM in emulsion polymerization is to define an effective chain transfer constant,[25] which is significantly less than the chemically controlled value characteristic of solution and bulk polymerizations. This is not the most desirable method because the effective value will only apply to the particular system being studied.[19] Nevertheless, the approach is suitable here because our goal is to compare experiments with different CTA concentrations and the effective value will not be a function of the CTA concentration.[24,25] The chain transfer coefficient [$k_{tr,CTA}$ in eq. (2)] was multiplied by a constant factor in order to obtain an accurate prediction of the molecular weight in the experiment with the highest CTA concentration. This factor was fixed and used for all other simulations within that system. The adjustment factors were 0.007 for ICS the system and 0.02 for the CS system. These small values are not surprising, given that Nomura et al.[17] showed that the concentration of *n*-DM in the particles can be 2 orders of magnitude less than the equilibrium value. No other adjustable parameters were used, and the simulation conditions were entirely consistent within a given system. In all cases, the simulations predicted starve-fed polymerization kinetics, in agreement with the experimental data.

References

1. Durant, Y. G.; Sundberg, D. C. Polym React Eng 2003, 11, 379.
2. Dimonie, V. L.; Daniels, E. S.; Schaffer, O. L.; El-Aasser, M. S. In Emulsion Polymerization and Emulsion Polymers; Lovell, P. A.; El-Aasser, M. S., Eds.; Wiley: 1997; p 293.
3. Sundberg, D. C.; Cassassa, A. J.; Pantazopoulos, J.; Muscato, M. R.; Kronberg, B.; Berg, J. J Appl Polym Sci 1990, 41, 1425.
4. Winzor, C. L.; Sundberg, D. C. Polymer, 1992, 33, 3797.
5. Durant, Y. G.; Sundberg, D. C. J Appl Polym Sci 1995, 58, 1607.
6. Stubbs, J. M.; Karlsson, O. J.; Jönsson, J.-E.; Sundberg, E.; Durant, Y. G.; Sundberg, D. C. Colloids Surf A 1999, 153, 255.
7. Karlsson, L. E.; Karlsson, O. J.; Sundberg, D. C. J Appl Polym Sci 2003, 90, 905.
8. Stubbs, J. M.; Sundberg, D. C. J Appl Polym Sci 2004, 6, 1538.
9. Krywko, W. P.; McAuley, K. B.; Cunningham, M. F. Polym React Eng 2002, 10, 135.
10. Mills, M. F.; Gilbert, R. G.; Napper, D. H. Macromolecules 1990, 23, 4247.
11. de la Cal, J.; Urzay, R.; Zamora, A.; Forcada, J.; Asua, J. J Polym Sci Part A: Polym Chem 1990, 28, 1011.
12. Chern, C.; Poehlein, G. J Polym Sci Part A: Polym Chem 1987, 25, 617.
13. Chern, C.; Poehlein, G. J Polym Sci Part A: Polym Chem 1990, 28, 3055.
14. Stubbs, J. M.; Durant, Y. G.; Sundberg, D. C. Compt Rend Chim 2003, 6, 1217.
15. Stubbs, J. M.; Sundberg, D. C. J Polym Sci Part B: Polym Phys 2005, 43, 2760.
16. Uraneck, C. A.; Burleigh, J. E. J Appl Polym Sci 1965, 9, 1273.
17. Nomura, M.; Suzuki, H.; Tokunuga, H.; Fujita, K. J Appl Polym Sci 1994, 51, 21.
18. Ma, J. W.; Cunningham, M. F. Macromol Symp 2000, 159, 85.
19. Ma, J. W.; Cunningham, M. F. J Appl Polym Sci 2000, 78, 217.
20. Witty, T.; Cunningham, M. F. Polym React Eng 2003, 11, 519.
21. Mendoza, J.; de la Cal, J.; Asua, J. M. J Polym Sci Part A: Polym Chem 2000, 38, 4490.
22. Zubitor, M.; Mendoza, J. C.; de la Cal, J.; Asua, J. M. Macromol Symp 2000, 150, 13.
23. Zubitor, M.; Asua, J. M. Macromol Mater Eng 2001, 286, 362.
24. Dietrich, B. K. J Appl Polym Sci 1988, 36, 1129.
25. Gugliotta, L. M.; Salazar, A.; Vega, J. R.; Meira, G. R. Polymer 2001, 42, 2719.
26. Manders, B. G.; Morrison, B. R.; Klostermann, R. Macromol Symp 2000, 155, 53.
27. De Gennes, P.-G. Scaling Concepts in Polymer Physics; Cornell University Press: Ithaca, NY, 1979; p 223.
28. Stubbs, J. M.; Carrier, R.; Karlsson, O. J.; Sundberg, D. C. Prog Colloid Polym Sci 2003, 124, 131.
29. Karlsson, O. J.; Carrier, R. H.; Stubbs, J. M.; Sundberg, D. C. Polym React Eng 2003, 11, 589.
30. Hourston, D. J.; Song, M.; Hammiche, A.; Pollock, H. G.; Reading, M. Polymer 1997, 38, 1.
31. Hourston, D. J.; Song, M. J Appl Polym Sci 2000, 76, 1791.
32. Hourston, D. J.; Song, M.; Pang, Y. J Brazil Chem Soc 2001, 12, 87.
33. Swier, S.; van Mele, B. Polymer 2003, 44, 6789.
34. Paxton, P. R. J Colloid Interface Sci 1969, 31, 19.
35. Stubbs, J. M.; Durant, Y. G.; Sundberg, D. C. Langmuir 1999, 15, 3250.
36. Stubbs, J. M.; Sundberg, D. C. Polymer 2005, 46, 1125.
37. Okubo, M.; Yamada, A.; Matsumoto, T. J Polym Sci Polym Chem Ed 1980, 16, 3219.
38. Gilbert, R. G. Emulsion Polymerization: A Mechanistic Approach; Academic: London, 1995.
39. PerkinElmer. Step-Scan DSC Method; http://www.perkinelmer.com/ or http://las.perkinelmer.com/catalog/Product.aspx?ProductID=N537–0679; PerkinElmer: Wellesley, MA, 2006.
40. Brandrup, J.; Immergut, E. H.; Grulke, E. A., Eds. Polymer Handbook, 4th ed.; Wiley: New York, 1999.
41. Wu, S. Polymer Interface and Adhesion; Marcel Dekker: New York, 1982.
42. Karlsson, O. J.; Stubbs, J. M.; Karlsson, L. E.; Sundberg, D. C. Polymer 2001, 42, 4915.